A Glimpse of the Mandelbulb with Memory

Ramón Alonso-Sanz
Technical University of Madrid, ETSIA (Estadistica, GSC)
C. Universitaria. 28040, Madrid, Spain
ramon.alonso@upm.es

An exploratory study is made concerning the effect of memory of past states on the dynamics of a kind of triplex number iterative map. Particular attention is paid to the case of the map generating the so-called Mandelbulb set.

1. Mandelbrot and Mandelbulb

The Mandelbrot set [1] is a mathematical object constructed in the complex plane. It is defined as the set of those points $z \in \mathbb{C}$ for which the orbit of $(0, 0)$ under iteration of equation (1) is bounded:

$$z_{T+1} = z_T^n + z_c. \tag{1}$$

There is no three-dimensional analog of the two-dimensional space of complex numbers [2], so that a canonical three-dimensional Mandelbrot set does not exist. But in order to introduce the mathematical object studied here, let us consider the polar form of a complex number $z = (\rho, \theta)$, so that equation (1) becomes:

$$(\rho, \theta)_{T+1} = (\rho, \theta)_T^n + (\rho_c, \theta_c) \tag{2}$$

where it is

$$(\rho, \theta)^n = (\rho^n, n\theta). \tag{3}$$

The Mandelbulb [3] is a three-dimensional object constructed using spherical coordinates (ρ, θ, φ), using as the formula for the "n^{th} power" of a vector in $\mathbb{R}^3$ the extension of that in the complex plane given by equation (3). Thus,

$$(\rho, \theta, \varphi)^n = (\rho^n, \mathrm{n}\theta, \mathrm{n}\varphi). \tag{4}$$

The Mandelbulb is then defined as the set of those points $(\rho_c, \theta_c, \varphi_c)$ in $\mathbb{R}^3$ for which the orbit of $(0, 0, 0)$ under iteration of equation (5) is bounded:

$$(\rho, \theta, \varphi)_{T+1} = (\rho, \theta, \varphi)_T^n + (\rho_c, \theta_c, \varphi_c). \tag{5}$$

This paper will focus on the quadratic map ($n = 2$) in Section 3 and on the $n = 8$ model in Section 4. Figure 1 shows the $n = 8$ Man-

https://doi.org/10.25088/ComplexSystems.25.2.109

delbulb set, which exhibits a bulb-like structure with fractal surface detail and a number of "lobes." These features emerge, albeit at different degrees, as soon as $n > 3$. Figure 1 is taken from [4], together with [5] considered the "official" Mandelbulb websites. These sites also provide information on the Juliabulb, that is, the mathematical objects achieved by fixing the $(\rho_c, \theta_c, \varphi_c)$ point and allowing for the variation of $(\rho_0, \theta_0, \varphi_0)$. We will not consider the Juliabulb here.

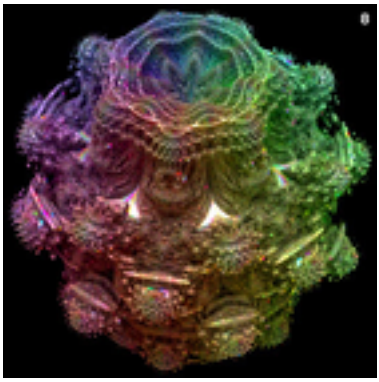

Figure 1. Nylander's $n = 8$ Mandelbulb set taken from [4].

2. Memory

The mapping of equation (5) may be endowed with explicit memory of past states in the form:

$$(\rho, \theta, \varphi)_{T+1} = \left(\overline{\rho}, \overline{\theta}, \overline{\varphi}\right)_T^n + (\rho_c, \theta_c, \varphi_c), \tag{6}$$

where the bars in the first summand of the second term indicate a mean value of the values achieved for every coordinate across the dynamics. This kind of memory implementation enables the explicit consideration of the memory of previous state values without altering the original form of the transition rule equation (5).

We will consider here the effect of average memory with geometric decay based on the memory factor α lying in the $[0, 1]$ interval:

$$\begin{aligned} \overline{\rho}_T &= \frac{\rho_T + \sum_{t=1}^{T-1} \alpha^{T-t} \rho_t}{\Omega(T)}, \qquad \overline{\theta}_T = \frac{\theta_T + \sum_{t=1}^{T-1} \alpha^{T-t} \theta_t}{\Omega(T)}, \\ \overline{\varphi}_T &= \frac{\varphi_T + \sum_{t=1}^{T-1} \alpha^{T-t} \varphi_t}{\Omega(T)}, \end{aligned} \tag{7}$$

where Ω stands for the sums of the factors considered; that is, $\Omega(T) = 1 + \sum_{t=1}^{T-1} \alpha^{T-t}$. The choice of the memory factor α simulates

https://doi.org/10.25088/ComplexSystems.25.2.109

the intensity of the memory effect: the limit case $\alpha = 1$ corresponds to a memory with equally weighted records (full memory), whereas $\alpha \ll 1$ intensifies the contribution of the most recent states (short-term memory). The choice $\alpha = 0$ leads to the ahistoric model. This kind of memory implementation will be referred to as α memory.

The length of the trailing memory may be limited to the last τ time steps. In the lowest length of memory scenario, that is, with $\tau = 2$, the equations (7) become:

$$\begin{aligned} \overline{\rho}_T &= \frac{\rho_T + \alpha\rho_{T-1}}{1+\alpha}, \qquad \overline{\theta}_T = \frac{\theta_T + \alpha\theta_{T-1}}{1+\alpha}, \\ \overline{\varphi}_T &= \frac{\varphi_T + \alpha\varphi_{T-1}}{1+\alpha}. \end{aligned} \tag{8}$$

Equations (9) show the general form of $\tau = 2$ memory implementation (referred to as ϵ memory, $0 \le \epsilon \le 1$):

$$\begin{aligned} \overline{\rho}_T &= \epsilon\rho_{T-1} + (1-\epsilon)\rho_T, \qquad \overline{\theta}_T = \epsilon\theta_{T-1} + (1-\epsilon)\theta_T, \\ \overline{\varphi}_T &= \epsilon\varphi_{T-1} + (1-\epsilon)\varphi_T. \end{aligned} \tag{9}$$

The memory models of equations (8) and (9) are interchangeable according to $\epsilon = \alpha / (1+\alpha)$ if $\epsilon \le 1/2$. The maximum memory charge under equation (8), that is, $\alpha = 1.0$, corresponds to $\epsilon = 0.5$, leading to the arithmetic mean of the last two state values. But levels of $\epsilon > 0.5$ allow for a higher contribution of the past than of the present state, which generates dynamics uncovered with $\tau = 2$ α memory.

This paper follows previous works on the effect of memory on real-valued discrete dynamical systems [6], on maps in the complex plane [7, 8], and on quaternionic maps [9, 10]. Incidentally, the quaternions, a noncommutative extension of the complex numbers to four dimensions, do not induce the rich variety of detail one might expect, given the detail seen in the conventional Mandelbrot set in $\mathbb{C}$. This might explain, at least to some extent, why some recent formulations (like the one treated in this paper) rely instead on manipulation of spatial coordinates in $\mathbb{R}^3$.

All the simulations in this paper are run up to $T = 1000$ or up to divergence, precisely up to ρ reaching the breakout value $\delta = 8.0$. Thus in the figures, red indicates the Mandelbrot set, blue indicates divergence at an even time step number, and white indicates divergence at an odd time step number.

Fortran code running with double precision in the mainframe mentioned in the Acknowledgments has been written to perform the computations in this paper. The code also generates the portable pixel maps (PPM) pattern images that are presented here in PDF format.

https://doi.org/10.25088/ComplexSystems.25.2.109

3. $n = 2$ Simulations

Figure 2 shows two-dimensional sections of the type $(x, y, 0)$, $(0, y, z)$, and $(x, 0, z)$ of the $n = 2$ Mandelbulb set with α and ϵ memories. The sections shown are parallel to the Cartesian axes and centered in the origin, with extent $[-1.5, 1.5]\times[-1.5, 1.5]$.

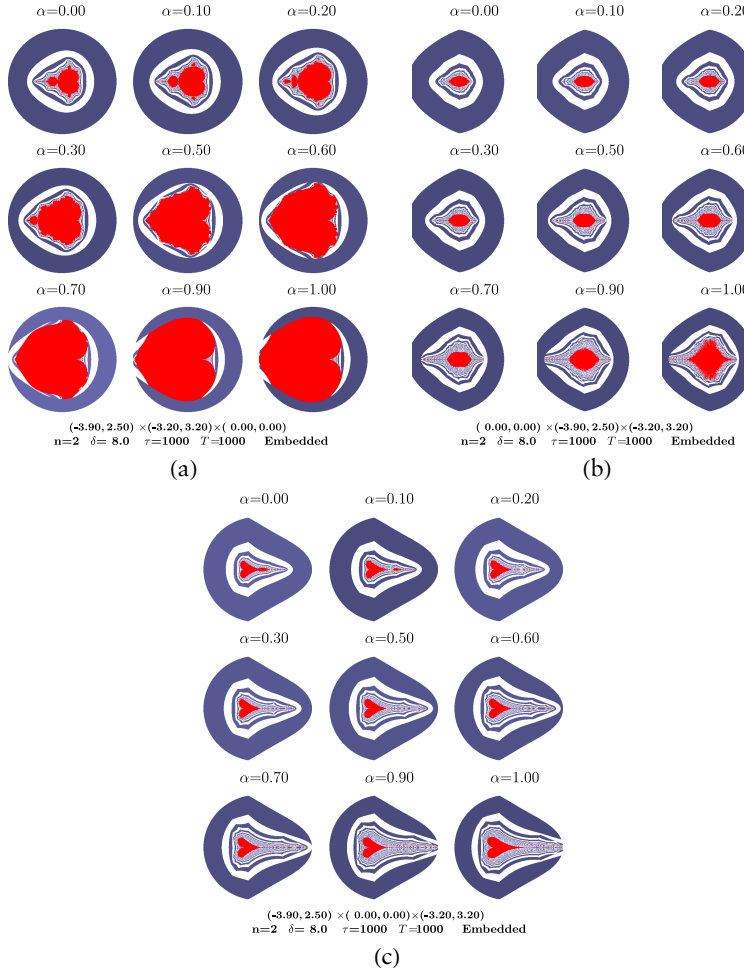

Figure 2. Three sections of the $n = 2$ Mandelbulb set with α memory. (a): $z = 0.0$; (b): $x = 0.0$; (c): $y = 0.0$. Color code: red → bounded pixels (Mandelbrot set); blue → divergence at an even time step number; white → divergence at an odd time step number.

The $(x, y, 0)$ sections shown in Figure 2(a) correspond to the effect of memory in the canonical two-dimensional Mandelbrot set M, a sce-

https://doi.org/10.25088/ComplexSystems.25.2.109

nario studied in [8]. As a result induced by the inertial effect that α memory exerts, M (top-left section in each frame, i.e., under $\alpha = 0.00$) grows in Figure 2 as α increases, so that it virtually occupies the region bounded by the outer blue band, which in turn is not very much altered, except on the left.

The effect of memory in the $(0, y, z)$ and $(x, 0, z)$ sections shown in Figure 2(a) and 2(c) is weaker than that exerted on the $(x, y, 0)$ section with respect to the growing of the bounded region (red). Besides, unlike in $(x, y, 0)$, the increase of α induces a notable effect in the proximity of the bounded region, even with $\alpha = 1.0$, in the $(0, y, z)$ and $(x, 0, z)$ sections.

The quadratic map in a three-dimensional context has been studied in [11, 12] using a kind of nondistributive scator algebra. Though this scenario differs from that of the triplex number studied here, the general form of the bounded region achieved with $n = 3$ according to equation (4) (not shown here) is reminiscent of that shown in [12].

3.1 Cartesian Coordinates

The map of equation (5) may be expressed in terms of Cartesian coordinates from the formulas that give the Cartesian coordinates from the spherical ones:

$$\begin{aligned} &x = \rho \cos\varphi \cos\theta, \qquad y = \rho \cos\varphi \sin\theta, \\ &z = \rho \sin\varphi. \end{aligned} \tag{10}$$

Thus, for $n = 2$ the formulas that give the Cartesian coordinates are:

$$\begin{aligned} \rho^2 &= \left(x^2 + y^2 + z^2\right)^2, \; x^2 + y^2 = \rho^2 \cos^2\varphi, \\ \sin^2\theta &= \frac{y^2}{\rho^2}\rho^2\cos^2\varphi = \frac{y^2}{x^2 + y^2}, \\ x^{(2)} &= \rho^2 \cos 2\varphi \cos 2\theta = \rho^2\left(1 - 2\sin^2\varphi\right)\left(1 - 2\sin^2\theta\right) = \\ &\rho^2\left(1 - 2\frac{z^2}{\rho^2}\right)\left(1 - 2\frac{y^2}{\left(x^2 + y^2\right)}\right) = \left(x^2 + y^2 - z^2\right)\frac{x^2 - y^2}{x^2 + y^2}, \\ y^{(2)} &= \rho^2 \cos 2\varphi \sin 2\theta = \rho^2\left(1 - 2\sin^2\varphi\right) 2\sin\theta\cos\theta = \\ &\rho^2\left(1 - 2\frac{z^2}{\rho^2}\right) 2\frac{x\,y}{\rho^2\cos^2\varphi} = 2\left(x^2 + y^2 - z^2\right)\frac{x\,y}{x^2 + y^2}, \\ z^{(2)} &= \rho^2 \sin 2\varphi = \rho^2\, 2\sin\varphi\cos\varphi = 2\rho^2\,\frac{z}{\rho}\sqrt{\frac{x^2 + y^2}{\rho}} = \\ &2\,z\sqrt{x^2 + y^2}\,. \end{aligned}$$

https://doi.org/10.25088/ComplexSystems.25.2.109

As a result, for $n = 2$ we have:

$$\begin{aligned} x_{T+1} &= \left(x_T^2 - y_T^2\right)\left(1 - \frac{z_T^2}{x_T^2 + y_T^2}\right) + x_c, \\ y_{T+1} &= 2x_T y_T\left(1 - \frac{z_T^2}{x_T^2 + y_T^2}\right) + y_c, \\ z_{T+1} &= 2z_T\sqrt{x_T^2 + y_T^2} + z_c. \end{aligned} \tag{11}$$

In turn, the map of equation (11) becomes with memory:

$$\begin{aligned} x_{T+1} &= \left(\overline{x}_T^2 - \overline{y}_T^2\right)\left(1 - \frac{\overline{z}_T^2}{\overline{x}_T^2 + \overline{y}_T^2}\right) + x_c, \\ y_{T+1} &= 2\overline{x}_T\overline{y}_T\left(1 - \frac{\overline{z}_T^2}{\overline{x}_T^2 + \overline{y}_T^2}\right) + y_c, \\ z_{T+1} &= 2z_T\sqrt{\overline{x}_T^2 + \overline{y}_T^2} + z_c. \end{aligned} \tag{12}$$

The square root in the z component of equation (11) implies the possibility of considering its positive or negative value. Here we have taken the positive one, that is, the so-called positive z component variation in [4]. The reader unfamiliar with hypercomplex numbers should also be warned that the formulas for the square of (x, y, z) in equation (11) are not achieved by squaring the quaternion (x, y, z, t) and projecting on the (x, y, z) subspace via $t = 0$. In fact, the formula is $\left(x + yi + zj + tk\right)^2 = \left(x^2 - y^2 - z^2 - t^2\right) + xyi + 2xzj + 2xtk$, so that making $t = 0$ gives $(x + yi + zj)^2 = \left(x^2 - y^2 - z^2\right) + 2xyi + 2xzj$. The latter is referred to as the quadratic formula in [13].

When n is odd, the equations (11) become rational polynomials in the three coordinates. Thus, for $n = 3$ the formula is:

$$\begin{aligned} z^{(2)} &= \rho^3 \sin 3\varphi = \rho^3 \sin\left(2\varphi + \varphi\right) = \\ &\rho^3\left(\sin\left(2\varphi\right)\cos\varphi + \cos\left(2\varphi\right)\sin\varphi\right) = \\ &2z\sqrt{x^2 + y^2}\,\sqrt{x^2 + y^2} + \left(x^2 + y^2 - z^2\right)z = z\left(3x^2 + 3y^2 - z^2\right). \end{aligned}$$

And consequently,

$$\begin{aligned} x_{T+1} &= x_T\frac{\left(3z_T^2 - \left(x_T^2 + y_T^2\right)\right)\left(x_T^2 - 3y_T^2\right)}{x_T^2 + y_T^2} + x_c, \\ y_{T+1} &= y_T\frac{\left(3z_T^2 - \left(x_T^2 + y_T^2\right)\right)\left(3x_T^2 - y_T^2\right)}{x^2 + y_T^2} + y_c, \\ z_{T+1} &= z_T\left(3\left(x_T^2 + y_T^2\right) - z_T^2\right) + z_c. \end{aligned} \tag{13}$$

https://doi.org/10.25088/ComplexSystems.25.2.109

Note that φ in equation (10) stands for the latitude (like in the usual geographic coordinate system). If φ stood for the colatitude, it would be:

$$x = \rho \sin\varphi \cos\theta, \qquad y = \rho \sin\varphi \sin\theta, \qquad z = \rho \cos\varphi. \tag{14}$$

The cosine variation in [4] based on the transformations in equation (14) makes a distorted-looking quadratic Mandelbulb set, but it yields nice-looking higher-order Mandelbulb sets [4]. Memory induces a much greater alteration on the Mandelbulb set achieved using the cosine variation compared to that shown here according to the transformations in equation (10).

4. $n = 8$ Simulations

This section deals with the most relevant n choice in the ahistoric model, that of $n = 8$. The figures in this section show two-dimensional sections of the three-dimensional long-term dynamics with α and ϵ memories.

Figures 3 and 4 show two-dimensional sections with one of the Cartesian coordinates equalized to zero. Contrary to the expectation from Section 3, the area of the bounded regions is not significantly altered with α memory in the sections of Figure 3. Neither is the form of the bounded region dramatically altered in Figure 3, albeit in the $(x, y, 0)$ scenario (Figure 3(a)) the seven isolated bulbs detectable in

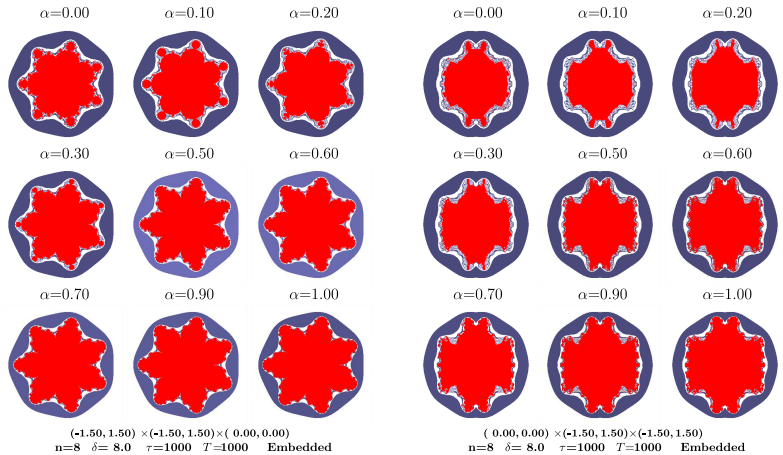

(a) (b)

Figure 3. (*continues*).

https://doi.org/10.25088/ComplexSystems.25.2.109

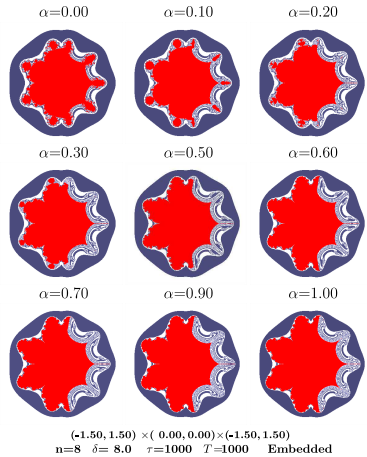

(c)

Figure 3. Three sections of the $n = 8$ Mandelbulb set with α memory. (a) $z = 0.0$; (b): $x = 0.0$; (c): $y = 0.0$. Color code as in Figure 2.

the ahistoric dynamics ($\alpha = 0$) merge with the core of the bounded region to generate a kind of hepta-star when $\alpha \geq 0.5$. In the $(x, 0, z)$ scenario (Figure 3(c)), a kind of shrink and drift to the left of the bounded region may be appreciated as α increases. The same conclusion is reached with ϵ memory in Figure 4, as the area and form of the bounded region are not notably altered as ϵ increases. Recall that the scenario of $\epsilon = 0.5$ coincides with that of τ=2 $\alpha = 1.0$ memory.

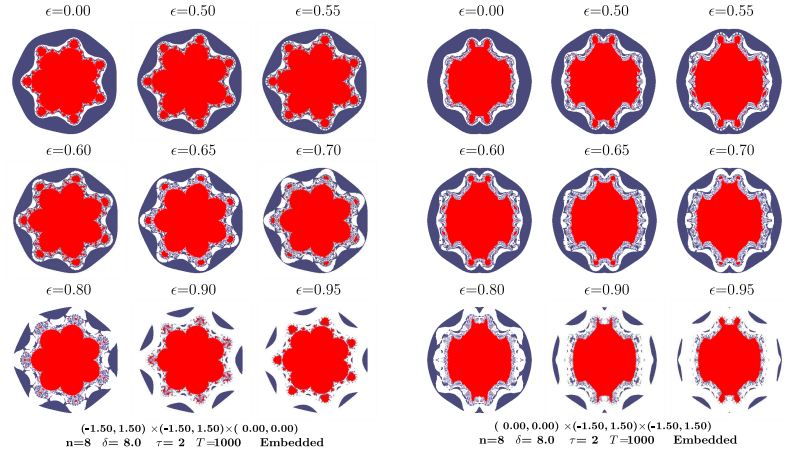

(a) (b)

Figure 4. (*continues*).

https://doi.org/10.25088/ComplexSystems.25.2.109

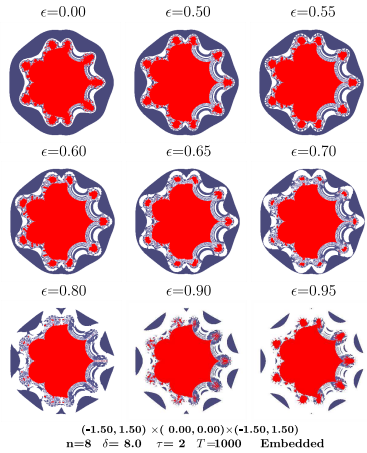

(c)

Figure 4. Three sections of the $n = 8$ Mandelbulb set with ϵ memory. (a): $z = 0.0$; (b): $x = 0.0$; (c): $y = 0.0$. Color code as in Figure 2.

Figures 5 and 6 show two-dimensional sections of the $n = 8$ Mandelbulb set with one of the Cartesian coordinates equalized to 0.5. The effect of memory in Figure 5 is comparable to that in Figure 3, though with particular characteristics, such as that the bulbs in the ahistoric dynamics in the $(x, y, 0)$ scenario (Figure 3(a)) become more enhanced (Figure 5(a)) instead of becoming merged with the core of the bounded region, and no drift is found in the $(x, 0, z)$ (Figure 5(c)) section. In turn, the effect of memory on Figure 6 is roughly

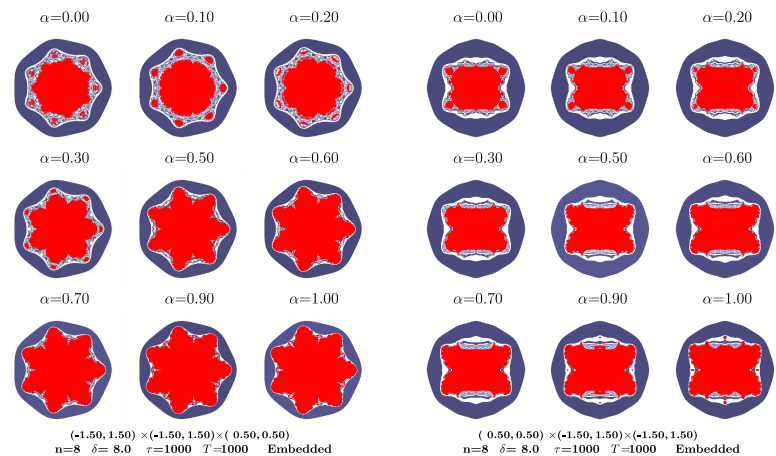

(a) (b)

Figure 5. (*continues*).

https://doi.org/10.25088/ComplexSystems.25.2.109

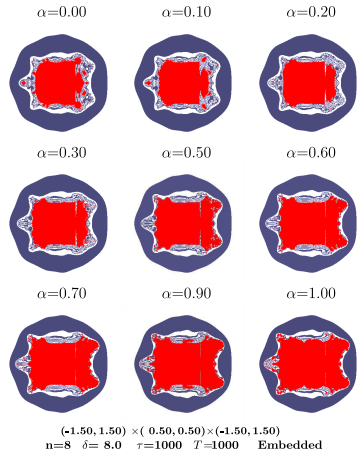

Figure 5. Three sections of the $n = 8$ Mandelbulb set with α memory. (a): $z = 0.5$; (b): $x = 0.5$; (c): $y = 0.5$. Color code as in Figure 2.

similar to that in Figure 4. In Figure 6, the values of ϵ in the $[0.5, 0.80]$ interval seem to preserve (or even increase) the complex behavior in the proximity of the bounded region. Let us call attention to the particular case in both Figure 4 and Figure 6 of $\epsilon = 0.7$, a memory factor close to the center of the $[0.5, 1.0]$ interval that weights the past more heavily than the last state value.

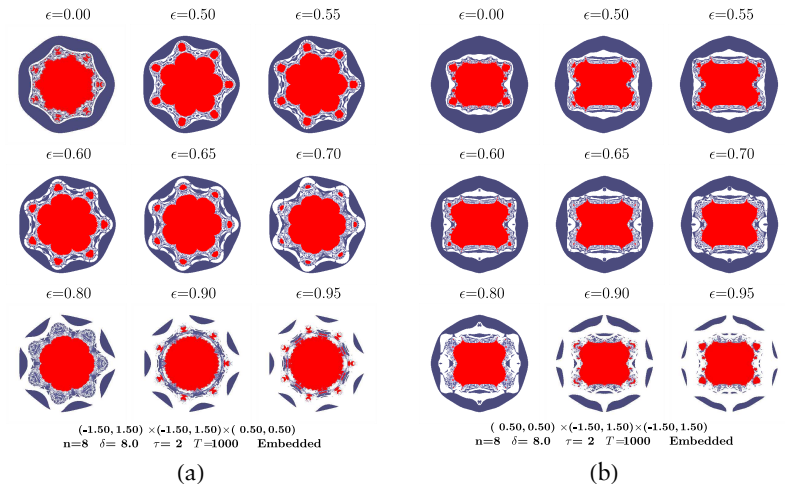

Figure 6. (*continues*).

https://doi.org/10.25088/ComplexSystems.25.2.109

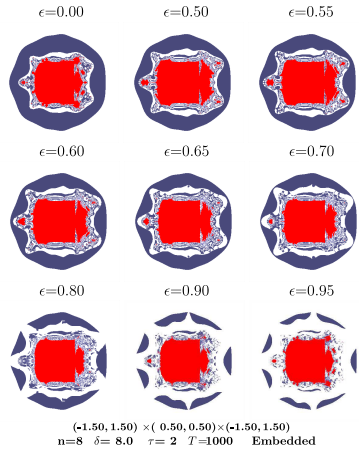

(c)

Figure 6. Three sections of the $n = 8$ Mandelbulb set with ϵ memory. (a): $z = 0.5$; (b): $x = 0.5$; (c): $y = 0.5$. Color code as in Figure 2.

Figures 7 and 8 show two-dimensional sections of the $n = 8$ Mandelbulb set with one of the Cartesian coordinates equalized to 1.0. Those are fairly outer sections, far from $(0, 0, 0)$, and consequently the areas of the bounded regions are small compared to those with the Cartesian coordinates equalized to 0.0 or to 0.5. In the case of the $x = 1.0$ section (top right) the bounded region is empty; that is, the section is out of the Mandelbulb set in the ahistoric dynamics,

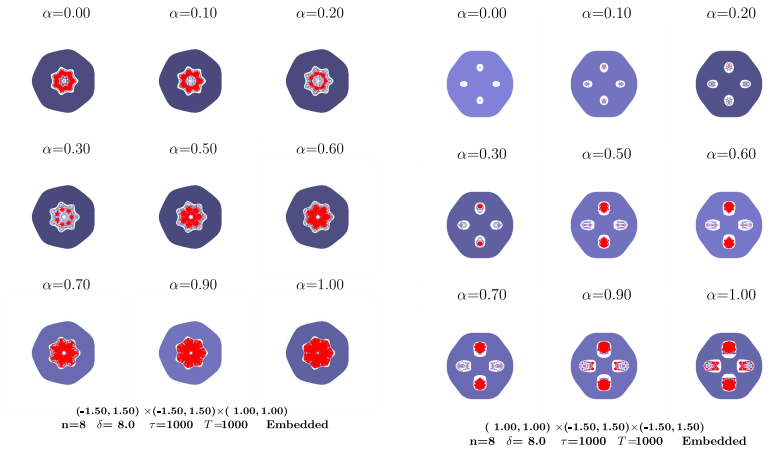

(a) (b)

Figure 7. (*continues*).

https://doi.org/10.25088/ComplexSystems.25.2.109

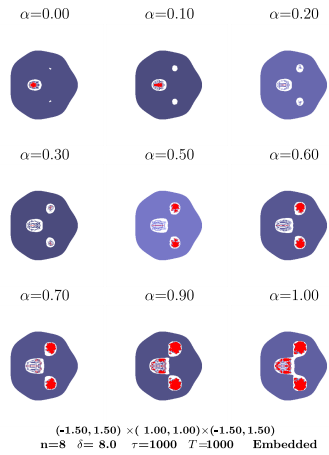

Figure 7. Three sections of the $n = 8$ Mandelbulb set with α memory. (a): $z = 1.0$; (b): $x = 1.0$; (c): $y = 1.0$. Color code as in Figure 2.

whereas with α memory (Figure 7), a few red-marked pixels appear as soon as $\alpha = 0.1$, increasing for higher values of this memory factor. The $x = 1.0$ section gets a nonempty bounded region in the $[0.5, 0.7]$ interval of ϵ in Figure 8.

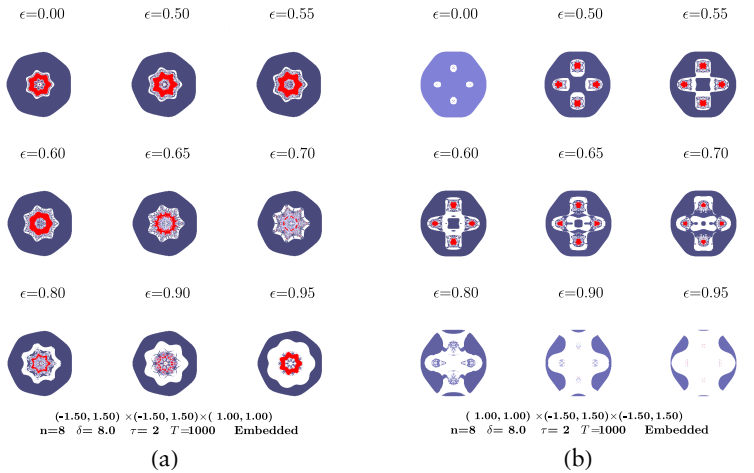

Figure 8. (*continues*).

https://doi.org/10.25088/ComplexSystems.25.2.109

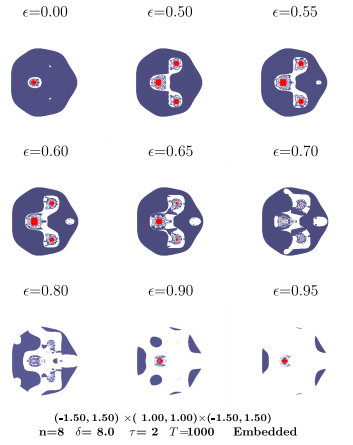

(c)

Figure 8. Three sections of the $n = 8$ Mandelbulb set with ϵ memory. (a): $z = 1.0$; (b): $x = 1.0$; (c): $y = 1.0$. Color code as in Figure 2.

4.1 Volume and Center of Gravity

As reported in the brief account given in [14], the Mandelbulb set is not mathematically well explored. Thus, for example, it seems to be connected like the Mandelbrot set, but this has not been mathematically proven yet. Even the simple issue of its volume has not been properly tackled so far. We have performed an estimation of the volume of the Mandelbulb by simple pixel counting. In the α memory scenario (Figures 3, 5, 7), that is, with the memory factor increasing as $\alpha = 0.0, 0.1, 0.2, 0.3, 0.5, 0.7, 0.9, 1.0$, the volume increases as $V = 2.256, 2.271, 2.315, 2.523, 2.962, 3.152, 3.334, 3.698, 3.951$. Whereas in the ϵ memory scenario (Figures 4, 6, 8), that is, with the memory factor increasing as $\epsilon = 0.0, 0.50, 0.55, 0.60, 0.65, 0.70, 0.80, 0.90, 0.95$, the volume varies as $V = 2.256, 2.690, 2.665, 2.593, 2.448, 2.298, 2.113, 2.100, 2.190$. The quadratic model gives a flat-looking Mandelbrot set (as may be seen in [4]). Memory induces its expansion as indicated by the increase of its volume in the context of Figure 2: $V = 0.278, 0.304, 0.332, 0.377, 0.583, 0.697, 1.245, 2.100, 2.349$. In the ϵ memory scenario (Figures 4, 6, 8), the notable growth of the volume in the Mandelbulb set with higher values of α is not apparent in the sections shown in Figure 2, particularly with respect to the $y = 0$ section.

Figure 9 graphs the increase of the volume of the Mandelbulb as a function of the memory charge α. The volumes reported in the preceding paragraph are plotted together with those for $\alpha = 0.4$ and $\alpha = 0.8$. The actual values of the volume are blue, and the fitted values are green. Figure 9(a) deals with the $n = 8$ scenario

https://doi.org/10.25088/ComplexSystems.25.2.109

of Figures 3, 5, 7, where the fitting equation plotted is $V(\alpha) = 2.256 + 0.7\alpha + 0.7\alpha^2$. This linear plus quadratic equation fits the volume for high memory charges ($\alpha \geq 0.8$) very well, albeit overestimates V for low alpha ($\alpha < 0.3$) and underestimates V for $0.3 < \alpha < 0.8$. Figure 9(b) deals with the $n = 2$ scenario of Figure 2, in which case the fitting equation $V(\alpha) = 0.278 + \alpha^2$ works very well up to $\alpha \leq 0.6$ but heavily underestimates V for $\alpha > 0.6$. Consequently, $V(\alpha) = 0.278 + \alpha^2 + \alpha$ has been adopted as the fitting equation for $\alpha > 0.6$ in Figure 9(b), as providing higher good estimations of V.

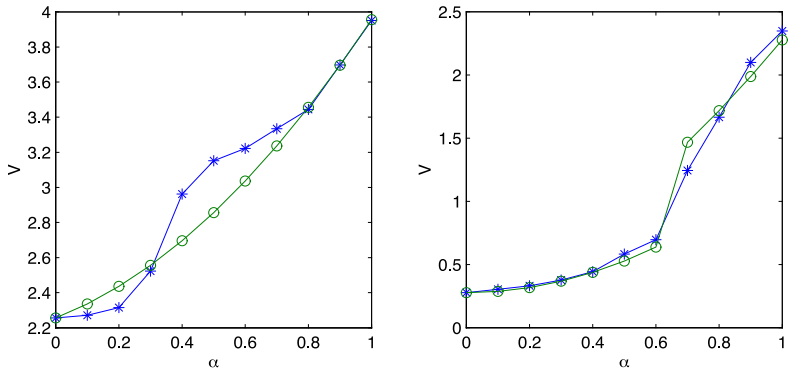

Figure 9. Volume of the Mandelbulb as a function of the memory charge α. Actual values are blue and fitted values (see text) are green. (a): $n = 8$ scenario of Figures 3, 5, 7. (b): $n = 2$ scenario of Figure 2.

The center of gravity of the $n = 8$ Mandelbulb set stays at $(0.0, 0.0, 0.0)$ in all the simulations run in this study, regardless of the memory types and charges implemented in them. In the $n = 2$ simulations reported in Figure 2, the x_g and z_g coordinates of the center of gravity stay at 0.0 regardless of memory, but its y coordinate varies as $y_g = -0.065, -0.048, -0.019, -0.019, 0.015, 0.044, 0.079, 0.175, 0.130$; thus, it slowly increases its value as α increases.

5. Conclusion and Future Work

This paper provides an initial exploratory study of the effect of memory of past states on the dynamics of triplex number iterative maps. Two-dimensional slices parallel to the xy, xz, and yz planes are shown in this study in order to assess the effect of memory in a fairly qualitative manner.

https://doi.org/10.25088/ComplexSystems.25.2.109

Further study of the effect of memory on triplex number iterative maps is due in at least two directions: (*i*) a more detailed scrutiny of the geometry, and (*ii*) mathematical foundation.

Concerning geometry, three-dimensional visualization [15–22] and printing [23] tools implementing ad hoc rendering and illuminating techniques need to be enriched to deal with memory. Once three-dimensional tools are available, the study of point trajectories will be feasible in graphic terms, so that a deeper study of technical aspects of the Mandelbulb with memory, such as the investigation of Misiurewicz points or the construction of an infinitely sized directed graph of points connected to other points, will be feasible.

The mathematical foundation task does not seem easy: nonlinear dynamics with memory in the hypercomplex space appears to demand, let us say, unconventional mathematics. Let us point out that fractional calculus has been applied in the analysis of discrete maps with memory [24]. Fractional calculus extends the definition of derivative and integral, allowing for noninteger orders. According to the Riemann–Liouville fractional approach, the definition of the integral of order α is reminiscent of the form of the equations (7), which is central to the application of fractional calculus to the study of systems with memory.

In another vein, the memory scheme adopted here may be altered in many ways. Let us mention two possible variants. First, the equations (5) may be endowed with memory in just one or two coordinates, not in the three implemented in equation (6). Thus, for example, with memory only in the ρ coordinate it would be:

$$(\rho, \theta, \varphi)_{T+1} = \left(\overline{\rho}, \theta, \varphi\right)_T^n + (\rho_c, \theta_c, \varphi_c). \tag{15}$$

Another variation may be that of computing the transition rule equation (5) first and then implementing memory of such points. Namely, to compute first:

$$(\rho^*, \theta^*, \varphi^*)_T = (\rho, \theta, \varphi)_T^n + (\rho_c, \theta_c, \varphi_c)$$

and then

$$(\rho, \theta, \varphi)_{T+1} = \left(\overline{\rho^*}, \overline{\theta^*}, \overline{\varphi^*}\right)_T.$$

These variants in memory implementation induce in turn particular alterations in the Mandelbulb set (as they do in the Mandelbrot set in the complex plane [7, 25]), which are to be examined in subsequent studies.

In the short term we plan to examine (with and without memory) the effect of convergence criteria alternative to those adopted to generate the Mandelbub set, that is, the Euclidean criterion $|\rho| < \delta$. In particular, we are interested in the convergence criterion adopted in the

https://doi.org/10.25088/ComplexSystems.25.2.109

so-called biomorphs [20, 26], based on the bounding of the coordinates, that is, either $|x| < \delta$, $|y| < \delta$, or $|z| < \delta$.

To the best of our knowledge, this kind of triplex number iterative map in equation (5) has not been properly studied in the academic context since its emergence in 2009. We hope that this paper might encourage the fractals community to investigate its properties, particularly those interested in three-dimensional fractals [27], as proper fractal features might emerge in the dynamics with memory. Of particular interest might be not necessarily adopting exactly the iterative mechanism of equations (4) and (5), but some of the variants of it presented in [4], such as, for example, the power n being a real number instead of an integer.

Acknowledgments

This work was supported by the Spanish grant MTM2015-6314-P. Part of the computations were performed on the HPC machine FISWULF, based on the International Campus of Excellence of Moncloa, funded by the UCM and FEDER funds.

References

[1] B. B. Mandelbrot, *The Fractal Geometry of Nature*, New York: W. H. Freeman, 1983.

[2] K. O. May, "The Impossibility of a Division Algebra of Vectors in Three Dimensional Space," *The American Mathematical Monthly*, **73**(3), 1966 pp. 289–291. doi:10.2307/2315349.

[3] J. Aron, "The Mandelbulb: First 'True' 3D Image of Famous Fractal," *New Scientist*, **204**(3736), 2009 p. 54.

[4] P. Nylander. "Hypercomplex Fractals." (Mar 30, 2016) http://www.bugman123.com/Hypercomplex.

[5] D. White. "The Unravelling of the Real 3D Mandelbulb." (Mar 30, 2016) http://www.skytopia.com/project/fractal/mandelbulb.html.

[6] R. Alonso-Sanz, *Discrete Systems with Memory*, Hackensack, NJ: World Scientific, 2011.

[7] R. Alonso-Sanz, "On Complex Maps with Delay Memory," *Fractals*, **23**(3), 2015 1550027. doi:10.1142/S0218348X15500279.

[8] R. Alonso-Sanz, "Scouting the Mandelbrot Set with Memory," *Complexity*, forthcoming. doi:10.1002/cplx.21632.

https://doi.org/10.25088/ComplexSystems.25.2.109

[9] R. Alonso-Sanz, "On Quaternion Maps with Memory," *Complex Systems*, **24**(3), 2015 pp. 223–233. http://www.complex-systems.com/pdf/24-3-2.pdf.

[10] S. Bedding and K. Briggs, "Iteration of Quaternion Functions," *The American Mathematical Monthly*, **103**(8), 1996 pp. 654–664. doi:10.2307/2974877.

[11] M. Fernández-Guasti, "Fractals with Hyperbolic Scators in 1 + 2 Dimensions," *Fractals*, **23**(2), 2015 1550004. doi:10.1142/S0218348X15500048.

[12] M. Fernández-Guasti, "An Intrinsically Three-Dimensional Fractal," *International Journal of Bifurcation and Chaos*, **24**(6), 2014 1430017. doi:10.1142/S0218127414300171.

[13] Wikipedia. "Mandelbulb." (Mar 30, 2016) https://en.wikipedia.org/wiki/Mandelbulb.

[14] O. Knill. "From the Sphere to the Mandelbulb." (Mar 30, 2016) http://www.math.harvard.edu/~knill/slides/boston/sic.pdf.

[15] J. Barrallo, "Expanding the Mandelbrot Set into Higher Dimensions," in *Proceedings of Bridges 2010: Mathematics, Music, Art, Architecture, Culture*, Pécs, Hungary (G. W. Hart and R. Sarhangi, eds.), 2010 pp. 247–254.

[16] R. Englund. "Rendering Methods for 3D Fractals." (Mar 30, 2016) http://www.diva-portal.org/smash/get/diva2:325566/FULLTEXT01.pdf.

[17] A. J. Hanson, *Visualizing Quaternions*, San Francisco: Morgan Kaufmann, 2006.

[18] J. C. Hart, D. J. Sandin, and L. H. Kauffman, "Ray Tracing Deterministic 3-D Fractals," *Computer Graphics*, **23**(3) 1989 pp. 289–296.

[19] A. Katunin and K. Fedio, "On a Visualization of the Convergence of the Boundary of Generalized Mandelbrot Set to $(n-1)$-Sphere," *Journal of Applied Mathematics and Computational Mechanics*, **14**(1), 2015 pp. 63–69. doi:10.17512/jamcm.2015.1.06.

[20] C. A. Pickover, *Computers, Pattern, Chaos and Beauty: Graphics from an Unseen World*, Mineola, NY: Dover Publications, 2001.

[21] I. Quilez. "Mandelbulb." (Mar 30, 2016) http://www.iquilezles.org/www/articles/mandelbulb/mandelbulb.htm.

[22] B. Rama and J. Mishra, "Generation of 3D Fractal Images for Mandelbrot Set," in *Proceedings of the 2011 International Conference on Communication, Computing, and Security (ICCCS '11)*, New York: ACM, 2011 pp. 235–238. doi:10.1145/1947940.1947990.

[23] O. Knill and E. Slavkovsky, "Illustrating Mathematics Using 3D Printers." arxiv.org/abs/1306.5599v1.

[24] V. E. Tarasov, *Fractional Dynamics: Applications of Fractional Calculus to Dynamics of Particles, Fields and Media*, Heidelberg, London: Springer, 2010.

https://doi.org/10.25088/ComplexSystems.25.2.109

[25] R. Alonso-Sanz, "The Mandelbrot Set with Partial Memory," *Complex Systems*, **23**(3), 2014 pp. 227–238.
http://www.complex-systems.com/pdf/23-3-2.pdf.

[26] C. A. Pickover, "Biom orphs: Computer Displays of Biological Forms Generated from Mathematical Feedback Loops," *Computer Graphics Forum*, **5**(4), 1986 pp. 313–316.
doi:10.1111/j.1467-8659.1986.tb00317.x.

[27] Fractal Forums. "Mandelbulb 3D."
http://www.fractalforums.com/mandelbulb-3d.

https://doi.org/10.25088/ComplexSystems.25.2.109